

STM contrast inversion of the Fe(110) surface

Gábor Mándi^a and Krisztián Palotás^{a,b,*}

^a*Budapest University of Technology and Economics,*

Department of Theoretical Physics, Budafoki út 8., H-1111 Budapest, Hungary

^b*Condensed Matter Research Group of the Hungarian Academy of Sciences,*

Budafoki út 8., H-1111 Budapest, Hungary

**Corresponding author, Email: palotas@phy.bme.hu, Tel: +3614634126*

(Dated: June 6, 2019)

Abstract

We extend the orbital-dependent electron tunneling model implemented within the three-dimensional (3D) Wentzel-Kramers-Brillouin (WKB) atom-superposition approach to simulate spin-polarized scanning tunneling microscopy (SP-STM) above magnetic surfaces. The tunneling model is based on the electronic structure data of the magnetic tip and surface obtained from first principles. Applying our method, we analyze the orbital contributions to the tunneling current, and study the nature of atomic contrast reversals occurring on constant-current SP-STM images above the Fe(110) surface. We find an interplay of orbital-dependent tunneling and spin-polarization effects responsible for the contrast inversion, and we discuss its dependence on the bias voltage, on the tip-sample distance, and on the tip orbital composition.

Keywords: STM imaging, SP-STM, orbital-dependent tunneling, spin-polarized tunneling, atomic contrast reversal, Fe(110)

PACS numbers: 72.25.Ba, 68.37.Ef, 71.15.-m, 73.63.-b

I. INTRODUCTION

The scanning tunneling microscope (STM) is a great equipment to study physical and chemical phenomena on a wide range of material surfaces in high spatial resolution. Its magnetic version, the spin-polarized STM (SP-STM) is one of the main tools for investigating atomic scale magnetism at material/vacuum interfaces [1] where the inversion symmetry is broken, giving rise to interesting magnetic phenomena. In order to explain relevant experimental findings on spin-polarized electron transport above magnetic surfaces, advanced and efficient theoretical methods are needed [2, 3]. Therefore, we propose a computationally efficient spin-polarized electron tunneling model based on the orbital-dependent atom-superposition approach [4] to simulate SP-STM where the electronic structure of the magnetic tip and surface is determined from first principles calculations. We apply the developed method to study the atomic contrast reversal on the Fe(110) surface.

Even in nonmagnetic STM, under certain bias voltage and tip-sample distance ranges, constant-current STM images can show atomic contrast inversion above flat metal surfaces, i.e., the apparent height of surface atoms can be smaller than that of the surface hollow position, and consequently, atoms do not always appear as protrusions on the STM images. This phenomenon was widely studied in the literature [4–7]. Chen theoretically explained the corrugation inversion found on low Miller index metal surfaces by the presence of $m \neq 0$ tip states [8]. For the particular case of the W(110) surface, Palotás et al. [4] highlighted the role of the real-space shape of the electron orbitals involved in the tunneling, including $m \neq 0$ tip states. On the other hand, Heinze et al. [6] pointed out that a competition between electron states from different surface Brillouin zone parts is responsible for the corrugation inversion effect. A similar explanation was given on the contrast inversion above the magnetic Fe(001) surface in the presence of an external electric field [9]. Following the real-space electron orbital picture, we expect that beside orbital-dependent effects [4] magnetic characteristics also play an important role in the determination of the corrugation quality of SP-STM images on magnetic surfaces. This expectation is supported by the reported bias voltage dependent magnetic contrast reversals in two different magnetic systems [10, 11] obtained by using spherical tunneling models. Note that the magnetic effect can be tuned in different ways, e.g., the magnetic contrast can be enhanced by properly adjusting the bias voltage and/or the tip magnetization direction [12], or by using chemically modified magnetic STM

tips [13].

In the present work we report the formalism capable of studying the interplay of orbital-dependent and spin-polarized tunneling effects within the three-dimensional (3D) Wentzel-Kramers-Brillouin (WKB) theory, and investigate the atomic contrast reversal on the Fe(110) surface.

II. SPIN-POLARIZED ORBITAL-DEPENDENT TUNNELING MODEL WITHIN THE 3D WKB THEORY

In SP-STM the total tunneling current can be written as the sum of a non-spin-polarized, I_{TOPO} , and a spin-polarized part, I_{MAGN} , i.e., $I_{TOT} = I_{TOPO} + I_{MAGN}$ [11, 14–17]. We combine this concept with the orbital-dependent electron tunneling model [4] within the 3D WKB framework based on previous atom-superposition theories [16–19]. Using the non-magnetic version of this orbital-dependent method provided comparable STM images of the W(110) surface with those obtained by standard Tersoff-Hamann [18, 20] and Bardeen [21] tunneling models implemented in the BSKAN code [3, 22]. The advantages, particularly computational efficiency, limitations, and the potential of the 3D WKB method were discussed in Ref. [23].

The model assumes that electron tunneling occurs through one tip apex atom only, and the transitions between this apex atom and a suitable number of sample surface atoms are superimposed [4, 24]. Since each transition is treated within the one-dimensional (1D) WKB approximation, and the 3D geometry of the tunnel junction is considered, the method is, in effect, a 3D WKB approach. The electronic structure of the magnetic tip and surface is included via the atom-projected electron density of states (PDOS) obtained by *ab initio* electronic structure calculations. Both the charge and magnetization PDOS are necessary to describe spin-polarized tunneling [11], and the orbital-decomposition of the PDOS is essential for the description of the orbital-dependent tunneling [4].

Assuming elastic tunneling and $T = 0$ K temperature, the non-spin-polarized (TOPO) and spin-polarized (MAGN) parts of the tunneling current measured at bias voltage V at

the \mathbf{R}_{TIP} tip position can be written as

$$I_{TOPO}(\mathbf{R}_{TIP}, V) = \int_0^V \frac{dI_{TOPO}}{dU}(\mathbf{R}_{TIP}, U, V) dU, \quad (1)$$

$$I_{MAGN}(\mathbf{R}_{TIP}, V) = \int_0^V \frac{dI_{MAGN}}{dU}(\mathbf{R}_{TIP}, U, V) dU. \quad (2)$$

The corresponding integrand can be written as a superposition of individual atomic contributions from the sample surface (sum over a):

$$\begin{aligned} & \frac{dI_{TOPO}}{dU}(\mathbf{R}_{TIP}, U, V) \\ &= \varepsilon^2 \frac{e^2}{h} \sum_a \sum_{\beta, \gamma} T_{\beta\gamma}(E_F^S + eU, V, \mathbf{d}_a) n_{S\beta}^a(E_F^S + eU) n_{T\gamma}(E_F^T + eU - eV). \end{aligned} \quad (3)$$

$$\begin{aligned} & \frac{dI_{MAGN}}{dU}(\mathbf{R}_{TIP}, U, V) \\ &= \varepsilon^2 \frac{e^2}{h} \sum_a \sum_{\beta, \gamma} T_{\beta\gamma}(E_F^S + eU, V, \mathbf{d}_a) \mathbf{m}_{S\beta}^a(E_F^S + eU) \mathbf{m}_{T\gamma}(E_F^T + eU - eV). \end{aligned} \quad (4)$$

Here, e is the elementary charge, h is the Planck constant, and E_F^S and E_F^T are the Fermi energies of the sample surface and the tip, respectively. The $\varepsilon^2 e^2/h$ factor gives the correct dimension (A/V) of the formal conductance-like dI/dU quantities [25]. The value of ε has to be determined by comparing the simulation results with experiments, or with calculations using more sophisticated methods, e.g., the Bardeen approach [21]. We chose $\varepsilon = 1$ eV [4] that gives comparable current values with those obtained from the Bardeen method. Note that the choice of ε has no qualitative influence on the reported results. $n_{S\beta}^a(E)$ and $n_{T\gamma}(E)$ are the orbital-decomposed charge PDOS functions of the a th sample surface atom and the tip apex atom with orbital symmetry β and γ , respectively. Similarly, $\mathbf{m}_{S\beta}^a(E)$ and $\mathbf{m}_{T\gamma}(E)$ are the corresponding energy-dependent magnetization PDOS vectors. These quantities are needed in Eqs.(3) and (4), respectively, and they can be obtained from a suitable electronic structure calculation. In collinear magnetic systems $n = PDOS^\uparrow + PDOS^\downarrow$ and $\mathbf{m} = m\mathbf{e}$ with $m = PDOS^\uparrow - PDOS^\downarrow$, where \mathbf{e} is the unit vector of the spin quantization axis [11]. The corresponding total charge or magnetization PDOS is the sum of the orbital-decomposed contributions: $n_S^a(E) = \sum_\beta n_{S\beta}^a(E)$, $n_T(E) = \sum_\gamma n_{T\gamma}(E)$, $\mathbf{m}_S^a(E) = \sum_\beta \mathbf{m}_{S\beta}^a(E)$, $\mathbf{m}_T(E) = \sum_\gamma \mathbf{m}_{T\gamma}(E)$. Note that a similar decomposition of the Green functions was employed within the linear combination of atomic orbitals (LCAO) framework in Ref. [5].

The sum over β and γ in Eqs.(3) and (4) denotes the superposition of the effect of atomic orbitals of the sample surface and the tip, respectively, via an orbital-dependent tunneling

transmission function: $T_{\beta\gamma}(E, V, \mathbf{d}_a)$ gives the probability of the electron tunneling from the β orbital of the a th surface atom to the γ orbital of the tip apex atom, or vice versa. The transmission probability depends on the energy of the electron E , the bias voltage V , and the relative position of the tip apex and the a th sample surface atom $\mathbf{d}_a = \mathbf{R}_{TIP}(x, y, z) - \mathbf{R}_a(x_a, y_a, z_a)$. In our model we consider $\beta, \gamma \in \{s, p_y, p_z, p_x, d_{xy}, d_{yz}, d_{3z^2-r^2}, d_{xz}, d_{x^2-y^2}\}$ atomic orbitals, and the following form for the transmission function:

$$T_{\beta\gamma}(E_F^S + eU, V, \mathbf{d}_a) = \exp\{-2\kappa(U, V)d_a\}\chi_\beta^2(\vartheta_a, \varphi_a)\chi_\gamma^2(\pi - \vartheta_a, \pi + \varphi_a). \quad (5)$$

Here, the exponential factor corresponds to an orbital-independent transmission where all electron states are considered as exponentially decaying spherical states [17, 18, 20], and it depends on the distance $d_a = |\mathbf{d}_a|$ and on the vacuum decay $\kappa(U, V) = \sqrt{2m[(\phi_S + \phi_T + eV)/2 - eU]}/\hbar$. We assume an effective rectangular potential barrier in the vacuum between the sample and the tip. ϕ_S and ϕ_T are the electron work functions of the sample surface and the tip, respectively, m is the electron's mass, and \hbar is the reduced Planck constant. The remaining factors of Eq.(5) are responsible for the orbital-dependence of the transmission function. They modify the exponentially decaying part according to the real-space shape of the electron orbitals involved in the tunneling, i.e., the angular dependence of the electron densities of the atomic orbitals of the surface and the tip is considered by the square of the real spherical harmonics $\chi_{\beta,\gamma}(\vartheta, \varphi)$. d_a , ϑ_a , and φ_a can be calculated for each surface atom from the actual tip-sample geometry: $d_a = \sqrt{(x - x_a)^2 + (y - y_a)^2 + (z - z_a)^2}$, $\vartheta_a = \arccos([z - z_a]/d_a)$, $\varphi_a = \arccos([x - x_a]/[d_a \sin \vartheta_a])$. For more details, please see Ref. [4].

From Eqs.(1)-(4) it is clear that the total tunneling current can be decomposed according to orbital symmetries: $I_{TOT}(\mathbf{R}_{TIP}, V) = \sum_{\beta,\gamma} I_{TOT}^{\beta\gamma}(\mathbf{R}_{TIP}, V)$. The absolute current contribution of the $\beta \leftrightarrow \gamma$ transition can be calculated as

$$I_{TOT}^{\beta\gamma}(\mathbf{R}_{TIP}, V) = \varepsilon^2 \frac{e^2}{h} \sum_a \int_0^V T_{\beta\gamma}(E_F^S + eU, V, \mathbf{d}_a) \times [n_{S\beta}^a(E_F^S + eU)n_{T\gamma}(E_F^T + eU - eV) + \mathbf{m}_{S\beta}^a(E_F^S + eU)\mathbf{m}_{T\gamma}(E_F^T + eU - eV)] dU, \quad (6)$$

while the relative contribution can be obtained as

$$\tilde{I}_{TOT}^{\beta\gamma}(\mathbf{R}_{TIP}, V) = \frac{I_{TOT}^{\beta\gamma}(\mathbf{R}_{TIP}, V)}{\sum_{\beta,\gamma} I_{TOT}^{\beta\gamma}(\mathbf{R}_{TIP}, V)}. \quad (7)$$

Note that the method can also be combined with arbitrary tip orientations [26] to study tip rotation effects on SP-STM images above magnetic surfaces, and an orbital-dependent atom-superposition model for the spin-polarized scanning tunneling spectroscopy (SP-STs) [24, 25] can also be developed.

III. RESULTS AND DISCUSSION

Using the presented spin-polarized orbital-dependent tunneling model, we study the atomic contrast reversal on the SP-STM images of the Fe(110) surface. We particularly focus on tip effects, and consider ideal magnetic tip models with different orbital symmetries, and a more realistic iron tip. The effect of three different tip magnetization orientations is also investigated. Based on convergence tests we choose 67 surface atoms involved in the atomic superposition for the Fe(110) surface, similarly as in Ref. [4] for W(110).

We performed geometry relaxation and electronic structure calculations within the generalized gradient approximation (GGA) of the density functional theory (DFT) implemented in the Vienna Ab-initio Simulation Package (VASP) [27–29]. A plane wave basis set for electronic wave function expansion in combination with the projector augmented wave (PAW) method [30] was applied, and the exchange-correlation functional is parametrized by Perdew and Wang (PW91) [31]. The electronic structures of the sample surface and the tip were calculated separately.

We model the Fe(110) surface by a slab of nine atomic layers with the experimental lattice constant of $a_{Fe} = 286.65$ pm. A separating vacuum region of 16.45 \AA width in the surface normal (z) direction has been set up between neighboring supercell slabs to minimize slab-slab interaction. After geometry relaxation the Fe-Fe interlayer distance between the two topmost layers is reduced by 7.8%, and the underneath Fe-Fe interlayer distance is reduced by 3.8% in comparison to bulk Fe. The size of the in-plane magnetic moment of the surface Fe atoms is $2.46 \mu_B$, in agreement with Ref. [6]. The unit cell of the Fe(110) surface (shaded area) and the rectangular scan area for the tunneling current simulations are shown in Figure 1 where the surface top (T) and hollow (H) positions are explicitly indicated. The average electron work function above the Fe(110) surface is $\phi_S = 4.73$ eV calculated from the local electrostatic potential. We used a $41 \times 41 \times 5$ Monkhorst-Pack [32] k-point grid for obtaining the orbital-decomposed projected charge and magnetization electron DOS onto

the surface Fe atom, $n_{S\beta}(E)$ and $\mathbf{m}_{S\beta}(E)$, respectively. The energy-dependent s , p , and d partial PDOS functions are shown in the left column of Figure 2. The d partial PDOS is clearly dominating in both cases, and there is a reversal of $m_{S,l=2(d)}(E)$ at about 0.6 eV below the Fermi energy. This is consistent with the calculations of Ref. [6] where the bottom of the minority surface state band was found at 0.7 eV below the Fermi level.

Within the presented spin-polarized orbital-dependent tunneling approach ideal magnetic tip models with particular orbital symmetries can be considered, i.e., γ_0 orbital symmetry corresponds to the energy-independent choice of $n_{T\gamma_0} = 1(\text{eV})^{-1}$ and $n_{T(\gamma \neq \gamma_0)} = 0$. Another characteristic for ideal magnetic tips is that their absolute spin polarization is maximal ($|P_T| = |m_T|/n_T = 1$) in the full energy range, i.e., combined with a particular γ_0 orbital symmetry: $\mathbf{m}_{T\gamma_0} = 1(\text{eV})^{-1}\mathbf{e}_T$ (\mathbf{e}_T is the unit vector of the tip spin quantization axis that is parallel to the assumed tip magnetization direction, an input parameter in our method) and $\mathbf{m}_{T(\gamma \neq \gamma_0)} = \mathbf{0}$. We took $\gamma_0 \in \{s, p_z, d_{3z^2-r^2}\}$ tip orbital symmetries. More realistic tips can be employed by explicitly calculating the orbital decomposition of the tip apex PDOS in model tip geometries. In the present work a blunt iron tip is used where a single Fe apex atom is placed on the hollow position of the Fe(001) surface [33]. The orbital-decomposed electronic structure data projected to the tip apex atom, $n_{T\gamma}(E)$ and $\mathbf{m}_{T\gamma}(E)$, were taken from Ref. [33] that were calculated by using the full potential linearized augmented plane wave (FLAPW) method. The s , p , and d partial PDOS functions are shown in the right column of Figure 2. The d partial PDOS is again dominating in both cases, and the reversal of $m_{T,l=2(d)}(E)$ occurs at about 0.8 eV below the tip Fermi energy. In the tunneling simulations we assumed a local electron work function of $\phi_T = 4.73$ eV above the tip apex.

The relative contributions of all $\beta \leftrightarrow \gamma$ orbital-dependent transitions to the total tunneling current, $\tilde{I}_{TO}^{\beta\gamma}$, can be calculated according to Eq.(7). Figure 3 shows representative histograms at different bias voltages and iron tip positions above the Fe(110) surface. We set the tip magnetization parallel to the in-plane Fe(110) surface magnetic moment. Parts a) and b) of Figure 3 correspond to the tip apex $z = 5 \text{ \AA}$ above the surface top (T) and hollow (H) positions, respectively (for T and H see Figure 1), and the bias voltage is set to $V = -0.1$ V. We find that the tip s (1) orbital provides the dominating contributions combined with the sample d_{yz} (6) and $d_{3z^2-r^2}$ (7) orbitals. The $d_{3z^2-r^2} - d_{3z^2-r^2}$ (7-7) transition also gives a sizeable contribution. The main difference between the T and H tip positions is that above the Fe(110) hollow site the $d_{yz} - d_{3z^2-r^2}$ (6-7 and 7-6) contributions gain, while the

$d_{3z^2-r^2} - d_{3z^2-r^2}$ (7-7) contribution loses weight, similarly to the finding above the W(110) surface [4]. This is due to the different orientational overlap of the mentioned tip and sample orbitals at the two tip positions, and it is not affected by the bias voltage. On the other hand, at a larger negative bias $V = -1.0$ V [Figure 3c) and 3d)] we observe that the tip s (1) orbital loses and the d_{yz} (6), $d_{3z^2-r^2}$ (7), and d_{xz} (8) orbitals and their tip-sample combinations gain weight. The largest contribution is now found for the $d_{3z^2-r^2} - d_{3z^2-r^2}$ (7-7) transition. We find an enhancement of this effect at $V = -2.0$ V [Figure 3e) and 3f)], and here the tip s (1) orbital contributions are tiny. This bias-trend can be explained by the surface and tip partial charge PDOS in Figure 2. At large negative bias voltages the combination of the surface occupied d partial PDOS with the tip unoccupied d partial PDOS clearly dominates over the tip s partial contributions. We find similar trends for a tip magnetization perpendicular to the surface, and also for positive bias voltages (consider the combination of the surface unoccupied with the tip occupied d partial charge PDOS in Figure 2).

As demonstrated in Ref. [4] the current difference between tip positions above the top (T) and hollow (H) surface sites is indicative for the corrugation character of a constant-current STM image. The total ($TOT = TOPO + MAGN$) current difference at tip-sample distance z and bias voltage V is defined as

$$\Delta I_{TOT}(z, V) = I_{TOT}^T(z, V) - I_{TOT}^H(z, V). \quad (8)$$

Positive ΔI_{TOT} corresponds to an STM image with normal corrugation where the atomic sites appear as protrusions, and negative ΔI_{TOT} to an inverted STM image with anticorrugation and atomic sites appearing as depressions. The $\Delta I_{TOT}(z, V) = 0$ contour gives the (z, V) combinations where the corrugation inversion occurs. Figure 4 shows such zero current difference contours calculated with four different tip models and three tip magnetization orientations in the $[-2 \text{ V}, +2 \text{ V}]$ bias voltage and $[0 \text{ \AA}, 14 \text{ \AA}]$ tip-sample distance range. Note that the validity of our tunneling model is restricted to about $z > 3.5 \text{ \AA}$. In Figure 4a), 4b), and 4c), a perpendicular, parallel, and antiparallel tip magnetization direction is respectively considered, compared to the Fe(110) surface magnetic moment. The perpendicular tip magnetization in Figure 4a) corresponds to a zero spin-polarized ($MAGN$) contribution of the current, thus $I_{TOT} = I_{TOPO}$, and solely orbital-dependent effects play a role in the tunneling without spin-polarization effects. Taking this case, for the ideal magnetic tips with specified orbital characters we find that the contrast inversion is shifted to larger tip-sample

distances in the full bias range following the order s , p_z , and $d_{3z^2-r^2}$, similarly as found for the W(110) surface [4]. This is due to the increasingly localized character of these tip orbitals in the z -direction. We expect normal corrugation above approximately 1.2 V (s -tip), 1.1 V (p_z -tip), and 1.0 V ($d_{3z^2-r^2}$ -tip) irrespective of the tip-sample distance. On the other hand, below the listed bias voltages there is a variance of the expected corrugation characters of the STM images in the $3.5 \text{ \AA} < z < 7 \text{ \AA}$ range depending on the tip orbital, but above 7 \AA anticorrugation is predicted for all considered ideal tips. Heinze et al. [6] calculated the bias-dependent corrugation at a fixed 4.5 \AA tip-sample distance with an s -tip. They reported a reversal from anticorrugation to normal one at 0.4 V by increasing the bias voltage. The same type of corrugation inversion is found by us in the positive bias range. Taking the iron tip having all nine orbital characters with weighted energy-dependent PDOS, anticorrugation is expected at short tip sample-distances $3.5 \text{ \AA} < z < 6 \text{ \AA}$ for all bias voltages. The [0.2 V, 0.8 V] bias interval provides corrugation inversion in the $z = 6\text{-}7 \text{ \AA}$ range, and outside this bias regime corrugation inversion occurs at higher tip-sample distances. It is clearly seen that the $\Delta I(z, V) = 0$ contours are considerably affected by the tip electronic structure.

In Figure 4b) the spin-polarized (*MAGN*) contribution of the current is non-zero due to the parallel magnetizations of the Fe(110) surface and the tip, and in this case both orbital-dependent and spin-polarization effects play a role in the tunneling. We observe that the quality of the $\Delta I_{TOT}(z, V) = 0$ contours changes considerably for the ideal magnetic tips compared to Figure 4a). With spin-polarized tunneling we expect normal corrugation above approximately 1.0 V (s -tip), 0.8 V (p_z -tip), and 0.6 V ($d_{3z^2-r^2}$ -tip) irrespective of the tip-sample distance. In the negative bias range, the contours are shifted to larger tip-sample distances, and below -0.6 V their shape is completely different from the ones in Figure 4a): For the contour obtained by the s -tip an increment of the tip-sample distance occurs. The p_z -tip provides interesting crossed contours at about -1.25 V and $z = 12 \text{ \AA}$. For the $d_{3z^2-r^2}$ -tip a regime with normal corrugation opens up below -1.0 V that does not depend on the tip-sample distance. The physical reason of these dramatic changes in the contours is the sign change of the d partial magnetization PDOS of the Fe(110) surface atoms (m_S) at 0.6 eV below the Fermi level, see Figure 2. Taking the iron tip we interestingly find that the quality of the corrugation inversion contours is practically unaffected by the spin-polarized tunneling. The largest difference is found in the [-1.2 V, -0.2 V] bias range in terms of

shifted tip-sample distances toward smaller values. This is due to the combined effect of the magnetic PDOS of the surface and the tip.

Figure 4c) shows $\Delta I_{TOT}(z, V) = 0$ contours calculated with a tip magnetization antiparallel to the Fe(110) surface magnetic moment. In this case the sign of the spin-polarized part of the current, I_{MAGN} , is reversed compared to the parallel tip magnetization scenario in Figure 4b). For the ideal tips the contours are almost the same in the positive bias range as in the non-spin-polarized tunneling case of Figure 4a), whereas for negative bias the contours are shifted to smaller tip-sample distances compared to the ones in Figure 4a) and b). Taking the iron tip we find that the contours are shifted to larger tip-sample distances by at least 1 Å in the [-1.2 V, -0.2 V] bias range compared to Figure 4a). These findings demonstrate the tunability of the height of the observable atomic contrast inversion depending on the spin-polarized tunneling and on the tip magnetization orientation.

In order to show the atomic contrast inversion more apparently, constant-current SP-STM images are simulated. We choose the iron tip and the bias voltage of $V = 0.25$ V, since the contrast inversion at this particular bias is expected at the shortest tip-sample distance of about $z = 5.8$ - 6.5 Å. The total tunneling current (I_{TOT}) was calculated in a box above the rectangular scan area shown in Figure 1 containing 707000 ($100 \times 70 \times 101$) grid points between 5.5 and 6.5 Å tip sample-distances with a 0.04 Å lateral and 0.01 Å vertical resolution. The constant-current contours are extracted following the method described in Ref. [11]. Figure 5 shows the simulated SP-STM images of the Fe(110) surface at seven different constant-current values and three magnetic orientations of the iron tip: perpendicular (first row: a-g), parallel (second row: h-n), and antiparallel (third row: o-u) to the Fe(110) surface magnetic moment. The current values (I) and the apparent heights of the Fe atom (z_{Fe}) are given in the caption of Figure 5. Going from the left to the right in Figure 5, the current value is decreasing with a concomitant movement of the tip farther from the surface. It can clearly be seen that the contrast inversion occurs as striped images at different tip heights depending on the tip magnetization orientation: perpendicular (d), parallel (i), and antiparallel (t). Note that in experiments the atomic resolution is lost close to the inversion [6]. Below the inversion we observe anticorrugation, i.e., the surface atoms appear as depressions, and above the inversion normal corrugation is obtained.

IV. CONCLUSIONS

We extended the orbital-dependent electron tunneling model implemented within the three-dimensional (3D) Wentzel-Kramers-Brillouin (WKB) atom-superposition approach to simulate spin-polarized scanning tunneling microscopy (SP-STM) above magnetic surfaces. Applying our method, we analyzed the bias-dependence of the orbital contributions to the tunneling current above the Fe(110) surface, and found a shift of the relevant tip s contributions close to zero bias toward $d-d$ tunneling at higher bias. We showed that spin-polarized tunneling has a considerable effect on the tip-sample distance where atomic contrast inversion occurs, and the tip magnetization direction plays a crucial role as well. We explained our results based on the sample and tip PDOS, and demonstrated the contrast inversion by simulating SP-STM images.

V. ACKNOWLEDGMENTS

The authors thank P. Ferriani and S. Heinze for providing the orbital-decomposed electronic structure data of the iron tip. Financial support of the Magyary Foundation, EEA and Norway Grants, the Hungarian Scientific Research Fund (OTKA PD83353, K77771), the Bolyai Research Grant of the Hungarian Academy of Sciences, and the New Széchenyi Plan of Hungary (Project ID: TÁMOP-4.2.2.B-10/1–2010-0009) is gratefully acknowledged. Furthermore, partial usage of the computing facilities of the Wigner Research Centre for Physics, and the BME HPC Cluster is kindly acknowledged.

-
- [1] R. Wiesendanger, *Rev. Mod. Phys.* 81 (2009) 1495.
 - [2] W. A. Hofer, A. S. Foster, and A. L. Shluger, *Rev. Mod. Phys.* 75 (2003) 1287.
 - [3] W. A. Hofer, *Prog. Surf. Sci.* 71 (2003) 147.
 - [4] K. Palotás, G. Mándi, and L. Szunyogh, *Phys. Rev. B* 86 (2012) 235415.
 - [5] N. Mingo, L. Jurczyszyn, F. J. Garcia-Vidal, R. Saiz-Pardo, P. L. de Andres, F. Flores, S. Y. Wu, and W. More, *Phys. Rev. B* 54 (1996) 2225.
 - [6] S. Heinze, S. Blügel, R. Pascal, M. Bode, and R. Wiesendanger, *Phys. Rev. B* 58 (1998) 16432.
 - [7] M. Ondráček, C. González, and P. Jelínek, *J. Phys. Condens. Matter* 24 (2012) 084003.

- [8] C. J. Chen, Phys. Rev. Lett. 69 (1992) 1656.
- [9] S. Heinze, X. Nie, S. Blügel, and M. Weinert, Chem. Phys. Lett. 315 (1999) 167.
- [10] R. Yang, H. Yang, A. R. Smith, A. Dick, and J. Neugebauer, Phys. Rev. B 74 (2006) 115409.
- [11] K. Palotás, W. A. Hofer, and L. Szunyogh, Phys. Rev. B 84 (2011) 174428.
- [12] K. Palotás, Phys. Rev. B 87 (2013) 024417.
- [13] W. A. Hofer, K. Palotás, S. Rusponi, T. Cren, and H. Brune, Phys. Rev. Lett. 100 (2008) 026806.
- [14] D. Wortmann, S. Heinze, P. Kurz, G. Bihlmayer, and S. Blügel, Phys. Rev. Lett. 86 (2001) 4132.
- [15] W. A. Hofer and A. J. Fisher, J. Magn. Magn. Mater. 267 (2003) 139.
- [16] A. R. Smith, R. Yang, H. Yang, W. R. L. Lambrecht, A. Dick, and J. Neugebauer, Surf. Sci. 561 (2004) 154.
- [17] S. Heinze, Appl. Phys. A 85 (2006) 407.
- [18] J. Tersoff and D. R. Hamann, Phys. Rev. B 31 (1985) 805.
- [19] H. Yang, A. R. Smith, M. Prikhodko, and W. R. L. Lambrecht, Phys. Rev. Lett. 89 (2002) 226101.
- [20] J. Tersoff and D. R. Hamann, Phys. Rev. Lett. 50 (1983) 1998.
- [21] J. Bardeen, Phys. Rev. Lett. 6 (1961) 57.
- [22] K. Palotás and W. A. Hofer, J. Phys. Condens. Matter 17 (2005) 2705.
- [23] K. Palotás, G. Mándi, and W. A. Hofer, Front. Phys. (2013) DOI: 10.1007/s11467-013-0354-4.
- [24] K. Palotás, W. A. Hofer, and L. Szunyogh, Phys. Rev. B 83 (2011) 214410.
- [25] K. Palotás, W. A. Hofer, and L. Szunyogh, Phys. Rev. B 85 (2012) 205427.
- [26] G. Mándi, N. Nagy, and K. Palotás (2013) arXiv:1307.4344.
- [27] G. Kresse and J. Furthmüller, Comput. Mater. Sci. 6 (1996) 15.
- [28] G. Kresse and J. Furthmüller, Phys. Rev. B 54 (1996) 11169.
- [29] J. Hafner, J. Comput. Chem. 29 (2008) 2044.
- [30] G. Kresse and D. Joubert, Phys. Rev. B 59 (1999) 1758.
- [31] J. P. Perdew and Y. Wang, Phys. Rev. B 45 (1992) 13244.
- [32] H. J. Monkhorst and J. D. Pack, Phys. Rev. B 13 (1976) 5188.
- [33] P. Ferriani, C. Lazo, and S. Heinze, Phys. Rev. B 82 (2010) 054411.

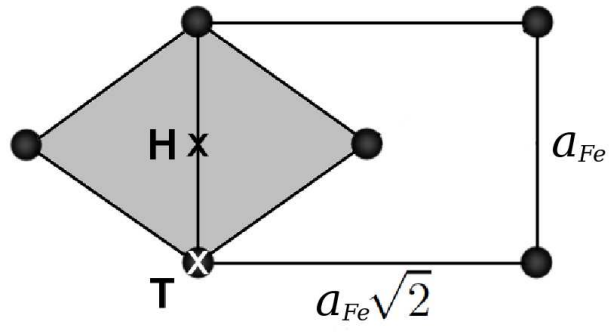


FIG. 1: The surface unit cell of Fe(110) (shaded area) and the rectangular scan area for the tunneling current simulations. Circles denote the Fe atoms. The top (T) and hollow (H) positions are explicitly shown.

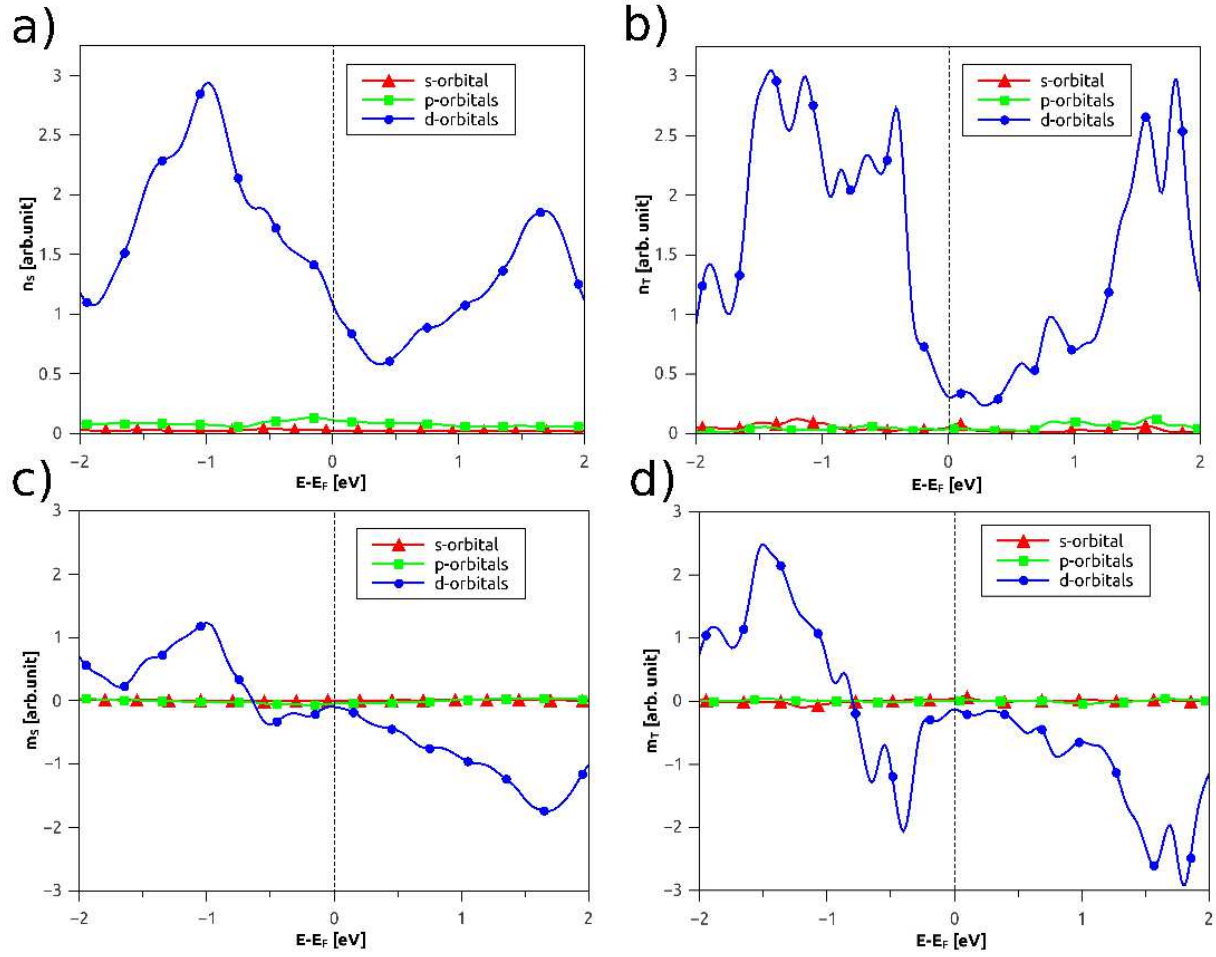


FIG. 2: (Color online) s , p , and d partial projected electron density of states (PDOS) of the Fe(110) surface atom and the iron tip apex atom. a) surface charge PDOS: $n_S(E)$; b) tip charge PDOS: $n_T(E)$; c) surface magnetization PDOS: $m_S(E)$; d) tip magnetization PDOS: $m_T(E)$.

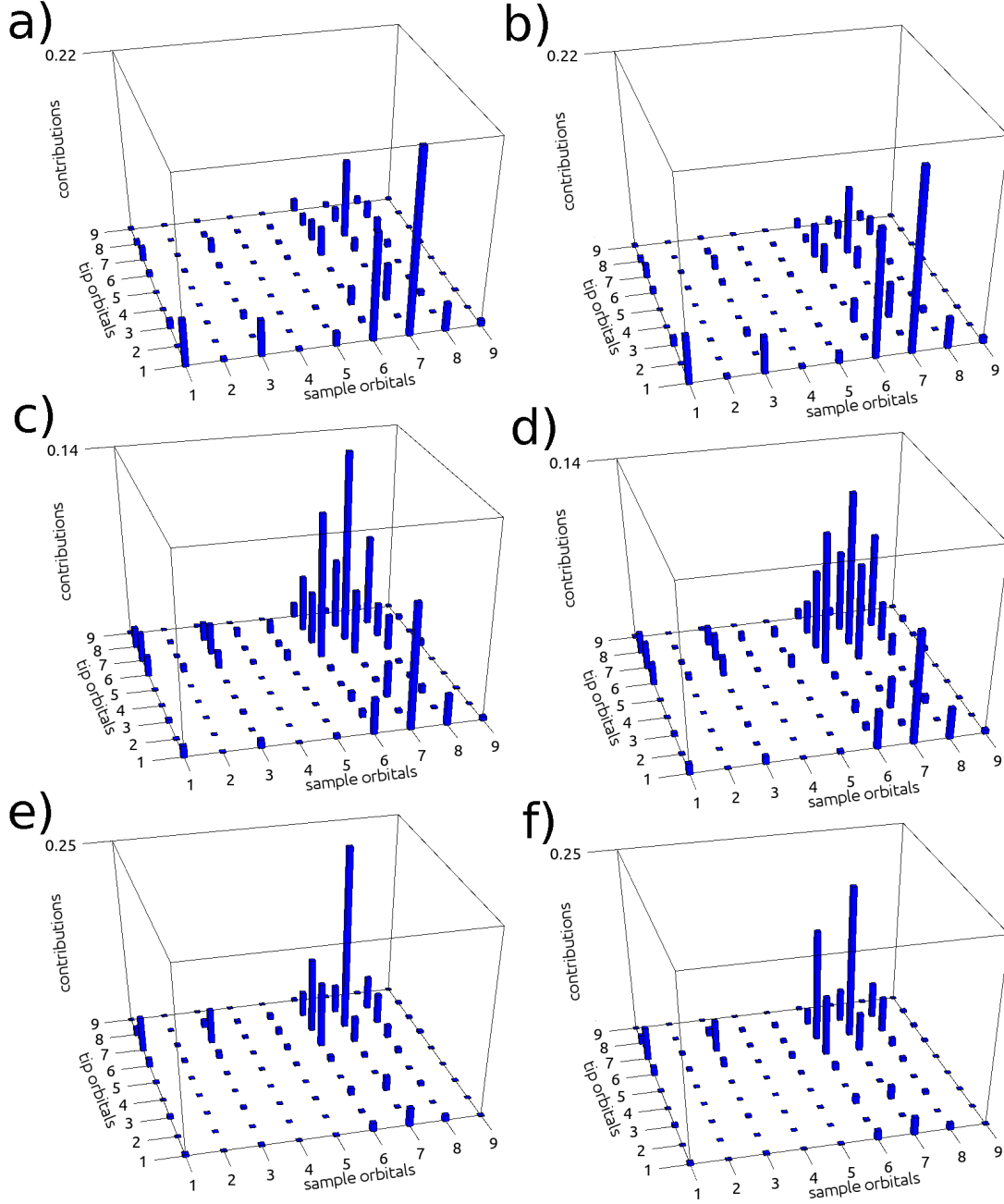


FIG. 3: (Color online) Histograms of the orbital-dependent relative current contributions $[\tilde{I}_{TOT}^{\beta\gamma}]$ in Eq.(7)] using the iron tip placed $z = 5 \text{ \AA}$ above two Fe(110) surface positions [top (T) and hollow (H), see Figure 1] at different bias voltages: a) T position, $V = -0.1 \text{ V}$; b) H position, $V = -0.1 \text{ V}$; c) T position, $V = -1.0 \text{ V}$; d) H position, $V = -1.0 \text{ V}$; e) T position, $V = -2.0 \text{ V}$; f) H position, $V = -2.0 \text{ V}$. The indices of the atomic orbitals (1-9) correspond to the order $\{s, p_y, p_z, p_x, d_{xy}, d_{yz}, d_{3z^2-r^2}, d_{xz}, d_{x^2-y^2}\}$.

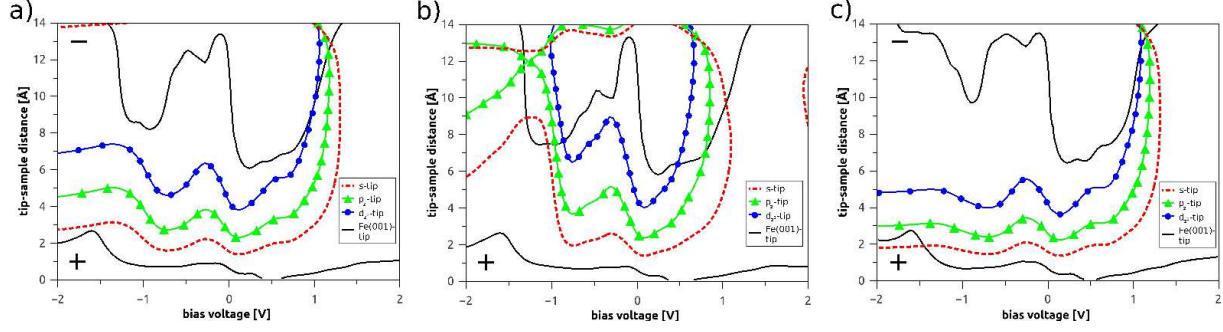


FIG. 4: (Color online) The $\Delta I_{TOT}(z, V) = I_{TOT}^T(z, V) - I_{TOT}^H(z, V) = 0$ contours indicative for the corrugation inversion [see Eq.(8), and its meaning in the text] calculated with four tip models above the Fe(110) surface. Parts a), b), and c) respectively correspond to perpendicular, parallel, and antiparallel tip magnetization orientations compared to the Fe(110) surface magnetic moment. The sign of ΔI_{TOT} (+ or -) is shown in selected (z, V) sections, and crossing the curve of the same tip-type inverts the sign. Note that positive ΔI_{TOT} corresponds to normal, while negative to inverted atomic contrast. For simplicity we used the notation d_{z^2} for $d_{3z^2-r^2}$.

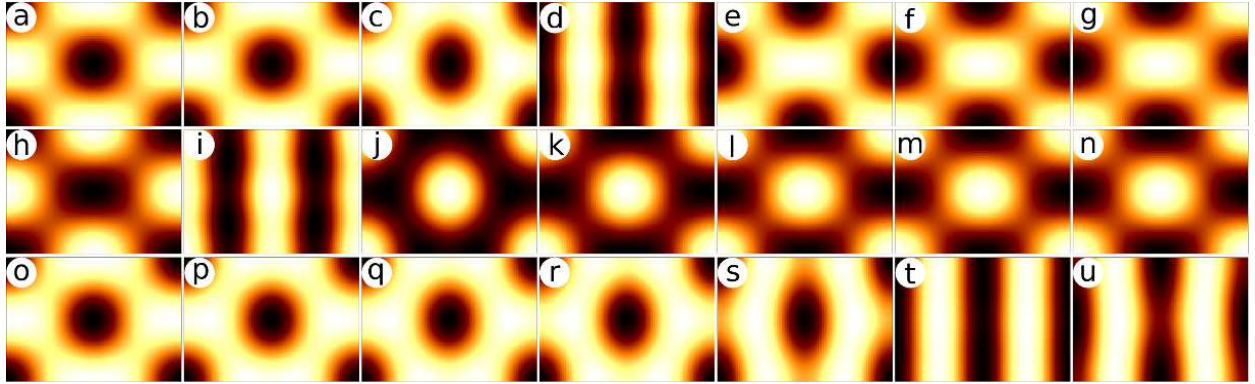


FIG. 5: (Color online) Simulated SP-STM images of the Fe(110) surface at $V = 0.25$ V bias voltage, at seven different constant-current values and three magnetic orientations of the iron tip: perpendicular (a-g), parallel (h-n), and antiparallel (o-u) to the Fe(110) surface magnetic moment. The current values (I) and the apparent heights of the Fe atom (z_{Fe}) are as follows: a), h), o) $I = 212$ pA, $z_{Fe} = 5.50$ Å; b), i), p) $I = 96$ pA, $z_{Fe} = 5.86$ Å; c), j), q) $I = 70$ pA, $z_{Fe} = 6.00$ Å; d), k), r) $I = 54$ pA, $z_{Fe} = 6.12$ Å; e), l), s) $I = 36$ pA, $z_{Fe} = 6.30$ Å; f), m), t) $I = 25$ pA, $z_{Fe} = 6.46$ Å; g), n), u) $I = 23$ pA, $z_{Fe} = 6.50$ Å. The SP-STM scan area corresponds to the rectangle shown in Figure 1. Light and dark areas denote larger and smaller apparent heights, respectively.